IOP Conference Series:
Materials Science and
Engineering

PURPOSE-LED
PUBLISHING™

PAPER • **OPEN ACCESS**

Defining Microstructural Features of Additively Manufactured Hot Work Steels and Predicting Mechanical Properties Using CNNs

To cite this article: A Khan *et al* 2026 *IOP Conf. Ser.: Mater. Sci. Eng.* **1350** 012030

View the article online for updates and enhancements.

You may also like

- The effect of processing parameters on dislocation density and tensile properties in laser powder bed fusion 316L
M Schreiber, C Brice, K Findley et al.
- Neutron diffraction analysis of microstructural evolution and mechanical behavior in an additively manufactured multiphase alloy
K Yamanaka, M Mori, Y Onuki et al.
- Selective Corrosion and Solidification Microstructure of Laser Powder Bed Fusion 316L Stainless Steel
Duane Armell Macatangay, Jenna Conrades, Keegan Brunner et al.

Enabling Electrochemistry
Inside and Outside the Lab

PalmSens

Discover our diverse range of Potentiostats engineered to support your research wherever it takes you

- Intuitive software for Windows and Android
- Proven in over 4000 scientific publications
- Single-channel and multi-channel
- Benchtop, portable and wearable

Discover More



This content was downloaded from IP address 134.130.185.37 on 06/11/2026 at 10:45

Defining Microstructural Features of Additively Manufactured Hot Work Steels and Predicting Mechanical Properties Using CNNs

A Khan[1,2]*, F Adjei-Kyeremeh[1], P Kowitwarangkul[2], S Richter[3], M Rom[4] and I Raffeis[1]*

[1]Foundry Institute, RWTH Aachen University, 52072 Aachen Germany.
[2]The Sirindhorn International Thai-German Graduate School of Engineering (TGGS-KMUTNB), North Bangkok, Thailand
[3]GFE, Central Facility for Electron Microscopy, RWTH Aachen University, 52072 Aachen Germany.
[4]Institute of Geometry and Applied Mathematics, RWTH Aachen University, 52072 Aachen Germany.

*E-mail: i.raffeis@gi.rwth-aachen.de
*E-mail: abdullahkhann2@rwth-aachen.de

Abstract. Additive manufacturing (AM) of hot work steels is challenged by complex interactions among process parameters, solidification conditions, alloy composition, and geometry, leading to non-equilibrium microstructures and property variations. These effects are particularly critical for alloys whose final properties depend on post-solidification phase transformations. This study investigates two hot work steels produced by laser powder bed fusion (PBF-LB) and direct energy deposition (DED-LB): the conventional H11 grade and a modified alloy designed for AM. Previously established PBF-LB microstructural and mechanical property datasets are combined with newly generated DED-LB results to comparatively evaluate microstructural evolution under different thermal processing conditions. Microstructural inhomogeneities—including cellular structures, phase distributions, and microsegregation—were analyzed under various pre- and post-heat treatment conditions, with emphasis on microsegregation evolution, precipitation behavior, and matrix transformations. The persistence or dissolution of cellular substructures strongly influences mechanical performance. Additionally, a previously developed convolutional neural network (CNN)-based approach was used for microstructure classification and prediction of yield and ultimate tensile strength from PBF-LB samples.

1. Introduction

Additive manufacturing (AM) processes impose rapid cooling and repeated thermal cycles that drive the microstructure far from equilibrium. For hot work tool steels, crack-free production becomes difficult when the desired final properties rely on martensitic transformation. Phases that form under conventional conditions may be suppressed or altered, leaving a supersaturated and thermodynamically unstable matrix. This metastable state, together with microsegregation and fine cellular substructures, strongly influences the response to subsequent heat treatments. Tempering can trigger secondary hardening, retained austenite decomposition, or carbide coarsening depending on the as-built microstructure. Understanding the interplay between initial AM-induced features and post-process thermal strategies is therefore essential for controlling strength, hardness, and toughness. In this work, we examine two laser-based AM processes:

Content from this work may be used under the terms of the Creative Commons Attribution 4.0 licence. Any further distribution of this work must maintain attribution to the author(s) and the title of the work, journal citation and DOI.
Published under licence by IOP Publishing Ltd

powder bed fusion (PBF) and directed energy deposition (DED). For PBF, a standard H11 tool steel was compared with a modified composition (H11m) under as-built, preheated, and several post-heat treatment conditions (see table 2). Tensile tests and microhardness measurements were used to evaluate mechanical performance. Exemplary PBF micrographs were used to train convolutional neural networks for classifying sample conditions and predicting strength properties, providing a fast data-driven complement to conventional testing. For DED, standard H11 was processed with analogous thermal treatments and hardness measured. Microstructural evolution, including cellular size, segregation, and carbide precipitation across treatments, was evaluated using SEM and EDS analysis.

2. Experimental Procedure

2.1 Powder Feedstock Characterization

Commercial gas-atomized H11 (1.2343) tool steel powder from Thyssenkrupp GmbH was used as the reference material. A modified version, H11m, was prepared by dry blending in a powder drum mixer. Table 1 lists the chemical compositions of both powders. For powder feedstock characterization, see [1].

Table 1. The alloy composition of H11 and H11m (wt.%).

Element	C	Si	Cr	Mo	Mn	V	Ni	Fe
H11	0.41	2.07	6.14	1.49	<0.01	0.46	–	bal.
H11m	0.38	2.06	5.61	1.19	1.11	0.41	3.07	bal.

2.2 PBF Processing and Post Processing

For detailed PBF processing parameters, please refer to [1]. The detailed post-heat treatment schedules are summarized in table 2. Metallographic specimens were prepared by standard grinding, polishing, and etching (3 % Nital). Microstructure was examined using a Zeiss LOM and a Zeiss Supra 55VP SEM with EDS. Microhardness (HV 0.5, DIN EN ISO 6507-1) and tensile tests (B4 specimens, DIN 50125) were performed on selected conditions using a Buehler MicroMet 5104 and an Instron 8033, respectively.

Table 2. Post-heat treatment schedules for H11 and H11m samples (as-built and preheated)

Code for Heat Treatment	Temperature (°C)	No. of Annealing Steps	Annealing Time (hours)
A	550	1	2
B	550	2	2×2*
C	550	1	4
D	550	2	2×4*
E	550	1	8
F	780	1	4

*2×2 and 2×4 represent two tempering cycles (each of 2h or 4h, respectively) with intermediate air cooling to room temperature between cycles.

2.3 DED Processing and Post Processing

Cuboid specimens (10×10×10 mm^3) were produced from the standard H11 powder using a LUNOVU iLMD system (LUNOVU GmbH, Germany). Argon served as both carrier and shielding gas. The deposition parameters were as follows: laser power of 1400 W, scanning speed of 1000 mm/s, laser spot diameter of 1.5 mm, and powder feed rate of 2.76 g/min. Samples were fabricated in both as-built and 400 °C substrate-preheated conditions, achieving relative densities above 99.5%. Post-build heat treatments, summarized in table 3, were applied to the as-built samples. Specimens were prepared and etched with Kalling's reagent. Microstructure and hardness were characterized using the same equipment as for the PBF samples.

Table 3. Post-heat treatment schedules applied to DED-fabricated H11 specimens.

Code	Heat Treatment Description	Temperature (°C)	Holding Time	Cooling Method
DT550	Direct tempering	550	2 × 2 h	Air Cooling
Q1010	Austenitizing + water quenching	1010	0.5 h	Water Cooling
QT550	Quenching + Tempering	550	2 × 2 h	Water/Air Cooling

3. Results and Discussion

Sample conditions are denoted as follows: S (standard H11), M (modified H11m), 0 (as-built, no preheating), P (preheated), and A–F refer to the post-heat treatment schedules listed in table 2.

3.1 Tensile Behavior of PBF-Processed Tool Steels

The yield strength (YS) and ultimate tensile strength (UTS) of the PBF processed H11 (standard) and H11m (modified) alloys were evaluated for selected heat treatment conditions. The results, reported in our earlier study [1], are illustrated in figure 1. The standard H11 and modified H11m demonstrated similar overall trends with increasing tempering time. Both alloys reached their highest strength levels after treatment B (two cycles of 2 h at 550 °C). Beyond this point, prolonged tempering (conditions D and E) resulted in a gradual decrease in YS and UTS.

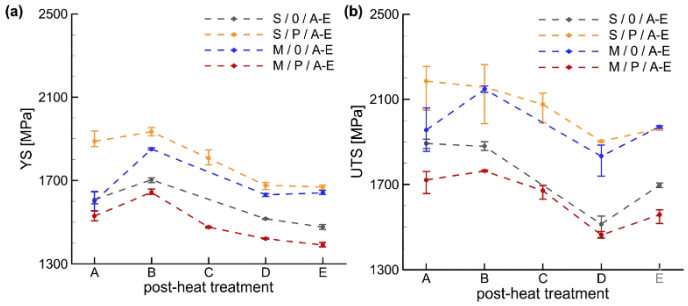


Figure 1. Effect of post-heat treatments (A–E) on (a) yield strength (YS) and (b) ultimate tensile strength (UTS) of LPBF-processed standard H11 (S) and modified H11m (M) in the as-built (0) and preheated (P) conditions. Adapted from [1].

3.2 Microhardness of PBF-LB/M and DED-LB/M Processed H11 Tool Steels

Microhardness (HV0.5) was measured on PBF-processed and DED-processed samples. PBF data are from our earlier study [2], while the DED results are reported here for the first time. The results revealed distinct responses of the additively manufactured H11 tool steels to processing conditions and post-heat treatments. In PBF processed samples, figure 2a, the modified H11m alloy yielded higher hardness than the standard H11 in the as-built condition (607 HV0.5 vs. 565 HV0.5). Substrate preheating at 500 °C produced the peak hardness values for both alloys (684 HV0.5 for standard H11 and 644 HV0.5 for modified H11m). Tempering at 550 °C (condition C) marginally increased standard H11 hardness (from 565 to 595 HV0.5) but marginally decreased modified H11m (from 607 to 585 HV0.5). In contrast, 780 °C (condition F) caused a sharp drop for both alloys, to 380 and 343 HV0.5, respectively. In contrast, DED processed standard H11 (figure 2b) exhibited a distinct hardness response. The as-built condition yielded 645 HV0.5, which decreased noticeably after preheating at 400 °C (495 HV0.5). Direct tempering at 550 °C (DT550) restored the hardness to 705 HV0.5, while austenitizing at 1010 °C followed by water quenching (Q1010) produced the highest value of 780 HV0.5. Subsequent tempering of the quenched material (QT550) reduced the hardness to 635 HV0.5.

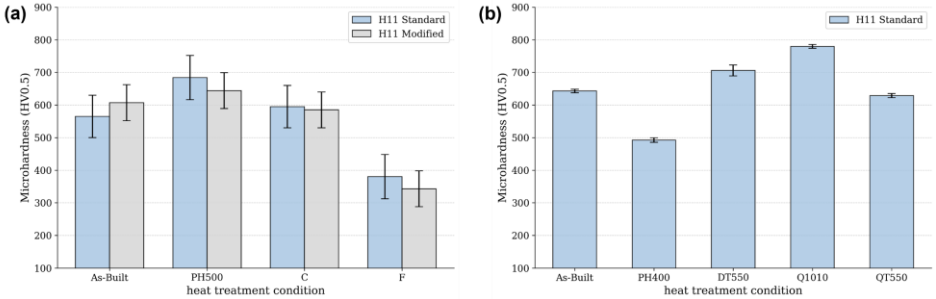


Figure 2. Microhardness (HV0.5) variation of H11 tool steel under different processing and post-heat treatment conditions: (a) PBF-processed standard H11 and modified H11m, adapted from [2]; (b) DED-processed standard H11 specimens. Error bars represent standard deviation calculated from five indentations per condition.

3.3 Microstructure–Property Relationships in PBF and DED Processed Hot Work Tool Steels

The mechanical properties of additively manufactured metals are not determined solely by the nominal alloy composition. Instead, they emerge from a complex interplay of process-specific thermal histories. Rapid cooling, remelting of previously deposited layers, steep thermal gradients, and in-situ reheating all influence solidification, microsegregation, and subsequent solid-state transformations. In this work, we examine two processes: laser powder bed fusion (PBF) and directed energy deposition (DED). Both produce characteristic cellular solidification structures, as reported earlier in previous studies [3,4,5]. However, cell size, microsegregation, retained austenite fraction, martensite lath dimensions, and carbide distribution all change with preheating and post-heat treatment. These microstructural variations are reflected in the observed differences in hardness and tensile strength.

In the as-built condition without preheating, **PBF-processed** standard H11 exhibits a well-defined cellular structure (figure 3a). Electron probe microanalysis (EPMA) reveals clear enrichment of chromium along the cell boundaries, indicating significant microsegregation of carbide-forming elements during rapid solidification (figure 3b). Further SEM and EDS analysis (figure 4a-d) is in agreement with this segregation pattern, illustrating a pronounced enrichment of carbide-forming elements such as Mo, Cr, and V along the cell boundaries. These decorated cell boundaries contribute to the composite-like strengthening of the martensitic matrix. Applying substrate preheating at 500 °C during PBF processing resulted in a different cellular morphology, with cell boundaries that appear less sharply defined (figure 3e). EPMA shows a more diffuse elemental distribution after preheating, indicating partial solute diffusion during the high-temperature hold. This reduces microsegregation and alters the local chemistry at cell walls. This reduction in microsegregation is consistent with the decrease in retained austenite from ≈18% in the non-preheated standard H11 to ≈1.1% after preheating, as reported in previous work [2]. The combination of reduced RA content and early fine carbide precipitation is consistent with the hardness increase observed in pre-heat samples for both H11 and H11m (figure 2a).

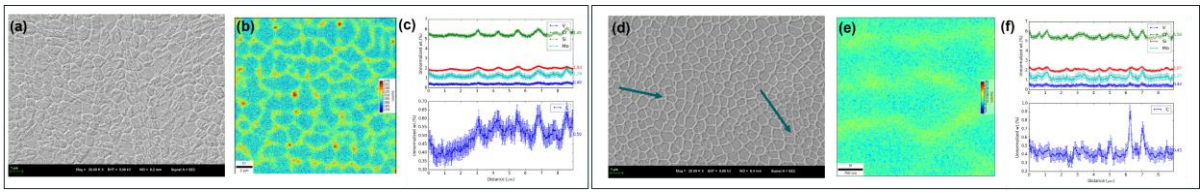


Figure 3. SEM and EPMA analysis of PBF-processed standard H11 alloy: (a–c) as-built condition (no pre-/post-heat treatment): (a) SEM image, (b-c) EPMA map and corresponding line scan, revealing a Cr-enriched cell-boundary network; (d–f) pre-heated condition (500 °C, as-built): (d) SEM image with arrows indicating precipitates, (e) EPMA map, exhibiting reduced segregation contrast at cellular boundaries; (f) EPMA line scan, revealing Cr enrichment along cellular boundaries.

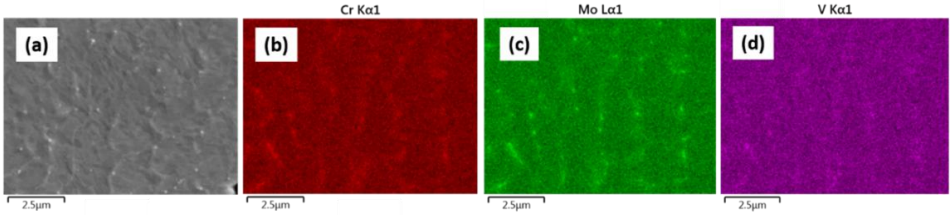


Figure 4. PBF-processed standard H11 (as-built, no preheat): (a) SEM image showing cell boundaries decorated with carbides; (b-d) EDS elemental maps revealing enrichment of Mo, Cr, and V along the cell boundaries. Adapted from [2].

While tempering at 550 °C (condition C) resulted in only marginal changes, treatment at 780 °C (condition F) caused a pronounced drop in hardness. This softening is widely ascribed to coarsening of secondary carbides and recovery of the martensitic matrix, as documented in the literature [3,6]. This trend is also reflected in the tensile properties (figure 1). The highest YS and UTS values were observed in the preheated standard alloy after double tempering (S/P/B).

Prolonging the tempering time (treatments C, D, and E) progressively reduced strength in both alloys. The SEM images of samples S/0/D and M/P/D (figure 5a,b) show a diffuse and discontinuous cellular network, with cell boundaries thinning and losing connectivity. The deterioration is even more severe in sample M/P/E (figure 5c), where no residual cellular structure remains. The observed strength loss after extended tempering is consistent with cell boundary degradation.

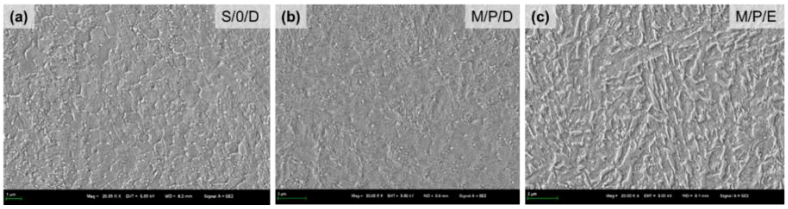


Figure 5. SEM images of PBF H11 after extended tempering: (a-b) S/0/D and M/P/D – partial cell boundary thinning; (c) M/P/E – complete loss of cellular structure (adapted from [1]).

A convolutional neural network (CNN) was applied to PBF-processed samples to automate microstructure classification and predict mechanical properties directly from SEM images. For CNN training, 25 sub-images (500 × 500 pixels) were extracted from each SEM image, resulting in 4135 images in total. Eighteen CNNs were trained with all images of 17 samples and then applied to the images of the remaining sample to assess generalizability. The CNNs contained six convolution layers comprising padding, convolution, batch normalization, ReLU activation, and max pooling, followed by two fully connected layers (one ReLU, one linear). For more details, we refer to [1]. The average prediction errors of the 18 CNNs are given in figure 6. The average mean absolute percentage error (MAPE) across all 18 samples was 4.1 % for YS and 3.9 % for UTS. These results demonstrate the potential of CNN-based analysis for extracting strength-relevant microstructural features from additively manufactured tool steels [1].

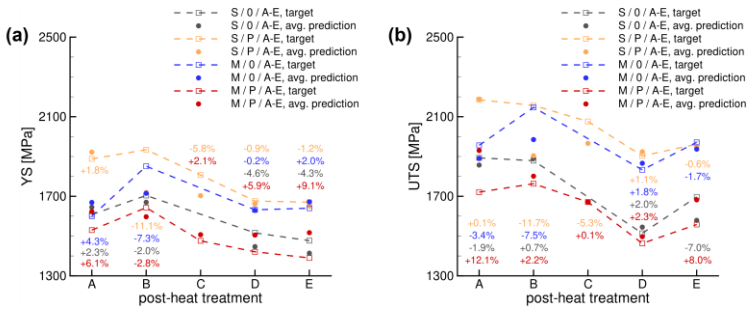


Figure 6: Averaged regression CNN predictions of (a) yield strength (YS) and (b) ultimate tensile strength (UTS) for all 18 sample conditions. Adapted from [1].

The **DED-processed** standard H11 displays a cellular solidification structure (figure 7a). EDS mapping (figure 7b–d) shows enrichment of Cr, V, and Mo along the cell boundaries. Higher-magnification BSE imaging (figure 7e) reveals carbide precipitates at a cell boundary, in agreement with the EDS maps (figure 7f–h) showing elevated concentrations of carbide-forming elements at these sites. Unlike PBF, substrate preheating at 400 °C during DED resulted in reduced hardness. This is attributed to the inherently greater heat accumulation and slower cooling rates in DED, where additional preheating likely promoted partial in-situ tempering during deposition, leading to matrix softening [6,7]. Direct double tempering at 550 °C (DT550) increased the hardness from 643 HV0.5 to 706 HV0.5. During tempering, matrix softening associated with recovery processes occurs concurrently with secondary hardening caused by fine secondary carbide precipitation. The observed hardness increase after DT550 is consistent with secondary hardening behavior commonly reported for additively manufactured H11/H13 tool steels tempered in this temperature range [3,4,6]. Compared to the quenched and tempered condition,

direct tempering preserves the as-built cellular substructure, which may promote finer secondary carbide precipitation during tempering. In contrast, prior austenitizing dissolves the as-built substructure and results in coarser carbide-rich regions (figure 8), reducing precipitation strengthening effectiveness and lowering hardness in the QT550 condition [6].

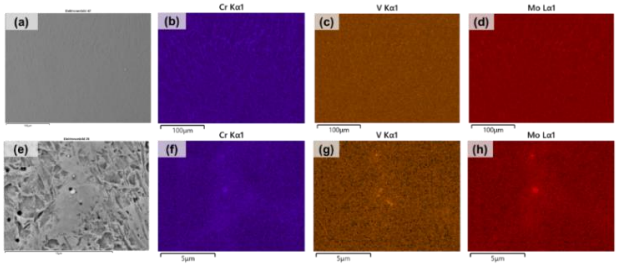


Figure 7. SEM and EDS analysis of DED-processed standard H11 (as-built condition): (a) SEM(SE) image showing the cellular solidification structure; (b–d) corresponding EDS maps revealing microsegregation of Cr, V, and Mo along the cell boundaries; (e) SEM(BSE) image at higher magnification showing carbides decorating a cell boundary; (f–h) EDS maps showing enrichment of carbide forming elements at these sites.

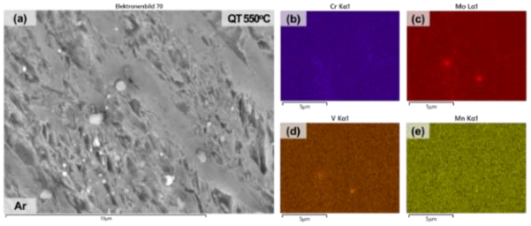


Figure 8: DED-processed standard H11 after quenching and tempering (QT550): (a) BSE-SEM micrograph showing coarsened carbide precipitation, and (b–e) corresponding EDS maps indicating elemental enrichment of Cr, Mo, V, and Mn.

4. Conclusion

The mechanical behavior of additively manufactured hot work tool steels depends strongly on process-specific thermal histories and non-equilibrium microstructures. In PBF, rapid solidification produced fine cellular martensitic structures with microsegregation and retained austenite. Preheating and optimized tempering reduced RA and stabilized cellular structures, enhancing hardness and strength, while prolonged tempering degraded the cellular network, causing softening. In DED, slower cooling gave a coarser cellular structure. Preheating at 400 °C reduced hardness, likely due to in-situ tempering. Direct tempering at 550 °C promoted secondary hardening, whereas quenching and tempering resulted in lower hardness because prior austenitizing dissolved the as-built substructure and promoted coarser carbides. A CNN trained on PBF micrographs distinguished 18 conditions and predicted YS and UTS with average MAPEs of 4.1 % and 3.9 %, showing that SEM images contain strength-relevant features. This combined approach offers a framework for tailoring microstructure and properties in additively manufactured hot work tool steels.

References

[1] Raffeis I, Rom M, Adjei-Kyeremeh F and Bührig-Polaczek A 2025 *Int. J. Adv. Manuf. Technol.* **140** 6249-6264
[2] Raffeis I, Adjei-Kyeremeh F, Ewald S, Schleifenbaum J H and Bührig-Polaczek A 2022 *J. Manuf. Mater. Process.* **6** 63
[3] Deirmina F, Peghini N, AlMangour B, Grzesiak D and Pellizzari M 2019 *Mater. Sci. Eng. A* **753** 109-121
[4] Casati R, Coduri M, Lecis N, Andrianopoli C and Vedani M 2018 *Mater. Charact.* **137** 50-57
[5] Huber F, Bischof C, Hentschel O, Heberle J, Zettl J, Nagulin K Y and Schmidt M 2019 *Mater. Sci. Eng. A* **742** 109-115
[6] Deirmina F, Amirabdollahian S, Lindwall G, Molinari A, Tiwari J K, Hryha E and Pellizzari M 2025 *Metall. Mater. Trans. A* **56** 88-110
[7] Ziesing U, Benito S, Weber S and Lentz J 2024 *J. Mater. Res. Technol.* **33** 4162–4175